2018

Elevated temperature dependence of the anisotropic visible-to-ultraviolet dielectric function of monoclinic β-Ga2O3

Alyssa Mock
University of Nebraska-Lincoln, alyssalynnmock@gmail.com

Jeremy VanDerslice
J. A. Woollam Co.

Rafal Korlacki
University of Nebraska-Lincoln, rkorlacki2@unl.edu

John A. Woollam
University of Nebraska-Lincoln, jwoollam1@unl.edu

Mathias Schubert
University of Nebraska - Lincoln, schubert@engr.unl.edu

Elevated temperature dependence of the anisotropic visible-to-ultraviolet dielectric function of monoclinic β–Ga_2O_3

A. Mock, J. VanDerslice, R. Korlacki, J. A. Woollam, and M. Schubert

Citation: Appl. Phys. Lett. **112**, 041905 (2018);
View online: https://doi.org/10.1063/1.5010936
View Table of Contents: http://aip.scitation.org/toc/apl/112/4
Published by the American Institute of Physics

Elevated temperature dependence of the anisotropic visible-to-ultraviolet dielectric function of monoclinic β-Ga_2O_3

A. Mock,[1,a)] J. VanDerslice,[2] R. Korlacki,[1] J. A. Woollam,[1,2] and M. Schubert[1,3,4]
[1]*Department of Electrical and Computer Engineering and Center for Nanohybrid Functional Materials, University of Nebraska-Lincoln, Lincoln, Nebraska 68588, USA*
[2]*J. A. Woollam Co., Inc., 645 M St. Lincoln Nebraska 68508, USA*
[3]*Leibniz Institute for Polymer Research, 01069 Dresden, Germany*
[4]*Terahertz Materials Analysis Center, Department of Physics, Chemistry and Biology (IFM), Linköping University, SE 58183 Linköping, Sweden*

(Received 27 October 2017; accepted 10 January 2018; published online 24 January 2018)

We report on the temperature dependence of the dielectric tensor elements of *n*-type conductive β-Ga_2O_3 from 22 °C to 550 °C in the spectral range of 1.5 eV–6.4 eV. We present the temperature dependence of the excitonic and band-to-band transition energy parameters using a previously described eigendielectric summation approach [A. Mock *et al.*, Phys. Rev. B **96**, 245205 (2017)]. We utilize a Bose-Einstein analysis of the temperature dependence of the observed transition energies and reveal electron coupling with average phonon temperature in excellent agreement with the average over all longitudinal phonon plasmon coupled modes reported previously [M. Schubert *et al.*, Phys. Rev. B **93**, 125209 (2016)]. We also report a linear temperature dependence of the wavelength independent Cauchy expansion coefficient for the anisotropic below-band-gap monoclinic dielectric tensor elements. *Published by AIP Publishing.* https://doi.org/10.1063/1.5010936

Recently, ultra-wide band-gap semiconductors with monoclinic crystal symmetry, β-Ga_2O_3, have become the subject of much research not only due to their potential for applications in transparent electronics and high-energy photonics but also due to their potential to replace GaN and SiC in next generation power electronics. The monoclinic β-phase of gallium oxide has the widest range of thermodynamic stability among the five polytypes (α, β, γ, δ, and ϵ).[1,2] Knowledge about the fundamental properties of semiconductors with monoclinic symmetry is not exhaustive. β-Ga_2O_3 is attracting attention because of a high electrical breakdown field of 8 MV/cm and a room-temperature electron mobility of 300 cm^2/Vs.[3–6] Schottky devices with reverse breakdown voltage in excess of 1 kV were reported.[7,8] The ultra-wide band-gap of β-Ga_2O_3 has been the topic of expanding computational and experimental work[9–14] and has been determined previously by ellipsometry techniques to have a value of 5.04 eV.[12] Ultra-violet solar-blind photodetectors have been reported.[15–17] Transparent devices with β-Ga_2O_3 may operate at elevated temperatures, and the temperature dependence of the properties of this emerging semiconductor is of interest. Recent combined investigations with generalized spectroscopic ellipsometry (GSE) and density functional theory (DFT) into the optical properties of this monoclinic semiconductor were made to explore the room temperature dielectric tensor element spectra and to identify electronic and excitonic properties in single crystalline β-Ga_2O_3.[12] Excitonic contributions were found to have distinct binding energies for different band pairs, unlike zincblende or wurtzite structure semiconductors, as a consequence of the highly anisotropic monoclinic lattice system. Also recently, the complete infrared active phonon mode properties were revealed by DFT and GSE investigations.[18] In particular, the coupling behavior of longitudinal optical (LO) modes with plasmon modes in *n*-type doped β-Ga_2O_3 was described and found to differ fundamentally from that of traditional semiconductor materials such as Si and GaAs. Longitudinal plasmon-phonon (LPP) modes were found to differ in their polarization directions from each other, and a strong dependence on the eigendielectric polarization directions on the charge carrier density was predicted. In a very recent paper, Sturm *et al.* report on the evolution of the dielectric function tensor in the visible-to-ultra-violet spectral regions from room temperature towards low temperatures. The dependence of the exciton and band-to-band transition was analyzed using the Bose-Einstein model.[19] In this work, we investigate the effect of elevated temperature onto the dielectric function of *n*-type doped β-Ga_2O_3 and derive therefrom excitonic and band-to-band transition energies using an eigendielectric polarization model approach.[12] In the eigendielectric polarization approach, critical point structures which contribute to the anisotropic dielectric function tensor of β-Ga_2O_3 are represented by direction dependent (dyadic) polarizability functions.[20] The direction dependence originates from the polarization selection rules of the interband matrix elements.[12] For monoclinic symmetry materials, an interesting question is whether and under what circumstance not only exciton and band-to-band transitions shift but whether their polarization selection rules change.

Two single side polished crystallographic surfaces, (010) and $(\bar{2}01)$, cut from a single crystal of Ga_2O_3 grown by Tamura Corp., Japan by edge-defined film fed growth process[21–23] were investigated. Mueller matrix spectroscopic ellipsometry data were collected in the spectral range of 194–1660 nm using a dual-rotating compensator ellipsometer (RC2, J. A. Woollam Co., Inc.). Samples were placed inside

a)Electronic mail: amock@huskers.unl.edu. URL: http://ellipsometry.unl.edu.

a nitrogen purged heating cell (Heat Cell, J. A. Woollam Co., Inc.) and aligned at an angle of incidence of 70°. Data were acquired *in-situ* while the sample chuck was heated from room temperature to 550 °C at a constant rate of 6 °C/s. The time to complete one measurement for one set of ellipsometry data (Mueller matrix element spectra) was approximately 10 s. Temperature dependent Mueller matrix data were collected from 3 azimuthal orientations per sample, by manually rotating each sample clockwise by sample normal in steps of approximately 45°. We note that window effects on the Mueller matrix elements were accounted for by utilizing a reference bulk Si wafer. All model calculations reported in this work were performed using WVASE32™ (J. A. Woollam Co., Inc.).

We choose a coordinate system as described in Ref. 12 with x parallel to **a**, y parallel to $\mathbf{c}^{\star}$, and z parallel to **b** yielding the dielectric tensor

$$\varepsilon = \begin{pmatrix} \varepsilon_{xx} & \varepsilon_{xy} & 0 \\ \varepsilon_{xy} & \varepsilon_{yy} & 0 \\ 0 & 0 & \varepsilon_{zz} \end{pmatrix}. \quad (1)$$

Note that $\mathbf{c}^{\star}$ is defined perpendicular to the **a**–**b** plane for convenience, while **c** shares the monoclinic angle $\beta = 103.7°$ with **a**.[24] A wavelength-by-wavelength approach is utilized at each temperature simultaneously fit to 6 independent datasets (2 samples with 3 orientations each) to obtain the dielectric tensor elements ε_{xx}, ε_{yy}, ε_{xy}, and ε_{zz}. We note that surface roughness was accounted for as described in Ref. 12. Critical point model functions are then projected into each direction as well as into the shear plane. From the parameters of these oscillator functions, amplitude, broadening, excitonic energy, transition energies, and their eigendielectric polarization orientation are determined. Details pertaining to this model approach can be found in Ref. 12.

Figure 1 depicts the real and imaginary parts of the dielectric function obtained at temperatures 22 °C, 50 °C, 100 °C, 150 °C, 200 °C, 250 °C, 300 °C, 350 °C, 400 °C, 450 °C, 500 °C, and 550 °C determined by a wavelength-by-wavelength approach. We observe a distinct broadening accompanied by a pronounced red-shift of the critical point features. To begin with, the below-band-gap dielectric tensor elements are analyzed, determining ε_{∞} for each non-vanishing tensor element. A Cauchy polynomial expansion was used retaining the first three coefficients in the wavelength expansion, augmented by a linear dependence on temperature for the wavelength independent Cauchy coefficient to analyze the wavelength-by-wavelength determined dielectric tensor elements

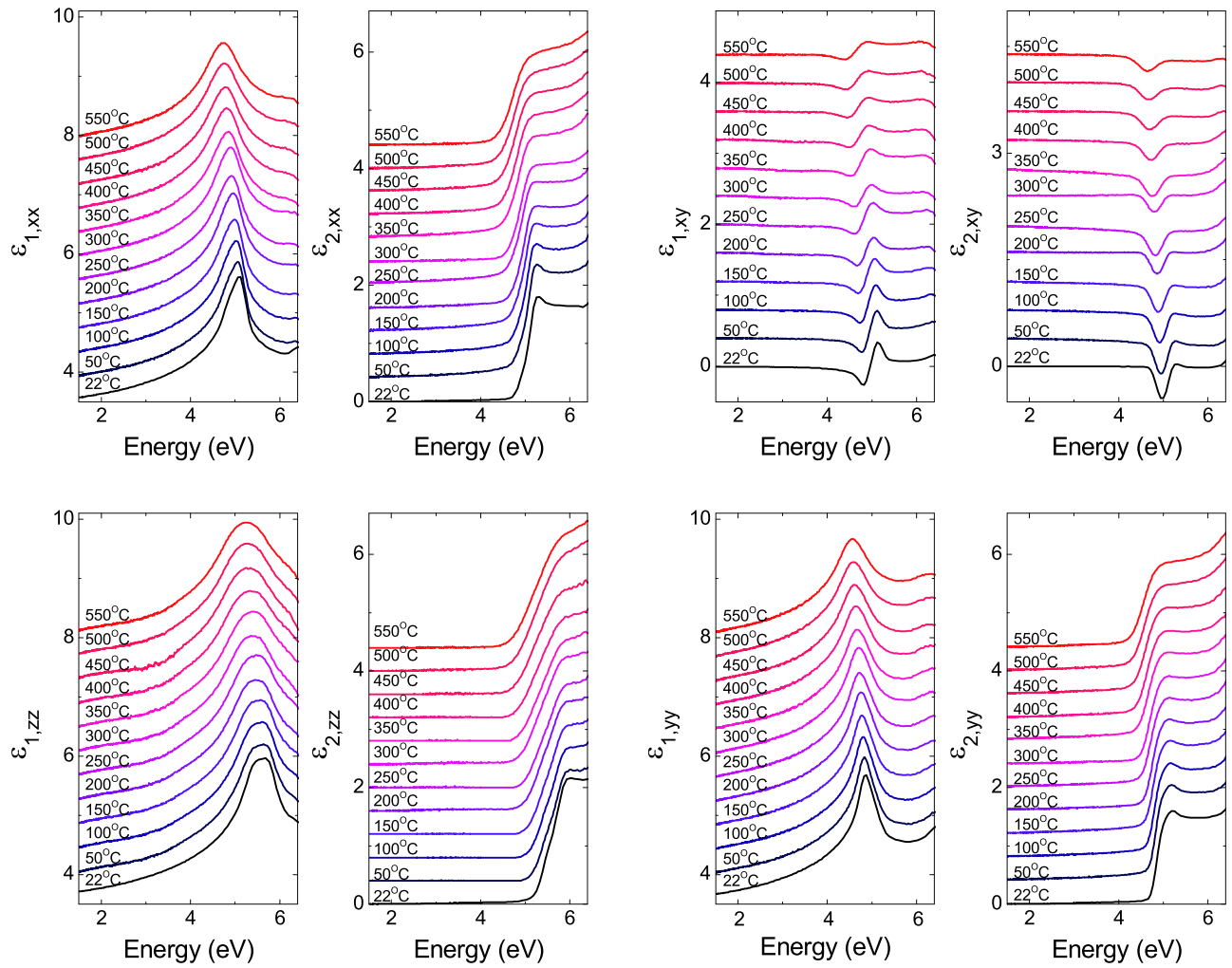

FIG. 1. Real and imaginary components of the dielectric tensor elements, ε_{xx}, ε_{yy}, ε_{xy}, and ε_{zz} for room temperature (black) to 550 °C (red). The functions were shifted vertically by increments of 0.4 with respect to each other for convenience.

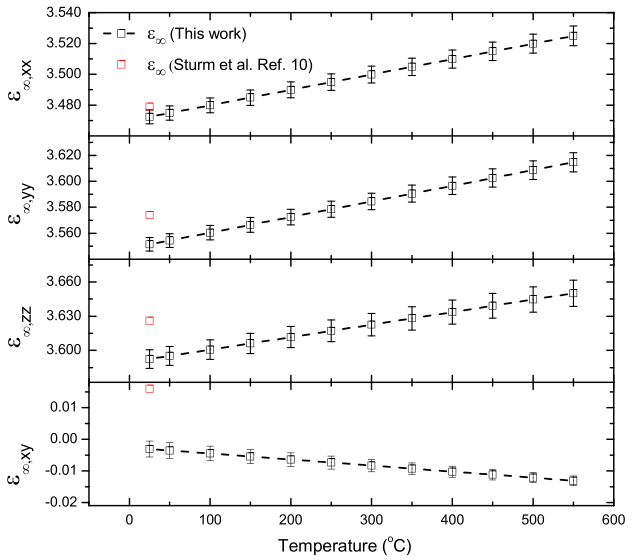

FIG. 2. Wavelength independent part (ε_∞) of the below-band-gap dielectric tensor elements of monoclinic β-Ga_2O_3 determined from the wavelength-by-wavelength extracted dielectric function tensor and a Cauchy polynomial wavelength expansion as a function of temperature (black squares), and the best-match linear interpolation (dashed lines).

$$\varepsilon_{1,ij} = \varepsilon_{\infty,ij} + A_{ij}(\mathrm{T} - \mathrm{T}_0) + \frac{B_{ij}}{\lambda^2} + \frac{C_{ij}}{\lambda^4}, \tag{2}$$

where T_0 is the room temperature. Figure 2 presents the best-match model parameter result for the wavelength independent portion of Eq. (2), obtained for each temperature investigated (black, boxes) and as a function of temperature (dashed lines). Table I lists all below-band-gap model parameters and compares ε_∞ values reported at room temperature previously (Sturm *et al.*, Ref. 10), where we note reasonable agreement except in the shear element ε_{xy}.

An eigendielectric displacement vector approach for model description of the dielectric function tensor in low-symmetry materials was described previously for the infrared spectral range (see Ref. 18 and references therein). Previously, we,[12] as well as Sturm *et al.*,[11] have utilized the eigendielectric displacement vector approach to describe electronic transitions and excitonic effects in β-Ga_2O_3 at room temperature. Here, we use the same approach as detailed in Ref. 12 for analysis of ellipsometry data measured at elevated temperatures and present model dielectric function parameters in Table II. Here, we present temperature-dependent changes to the critical-point (CP) transition energy model parameters only, for the lowest (CP_0^{ac}) and second-lowest (CP_0^{ac}) band-to-band transition polarized within the **a**–**c** plane, the lowest transition polarized parallel to the **b** direction (CP_0^b), and their excitonic partner contributions (CP_{0x}^{ac}, CP_{1x}^{ac}, CP_{0x}^b).[12] We note that amplitudes and broadening parameters follow a similar trend but are not included here. We observe that energy parameters decrease with increasing temperature. We note that due to broadening of critical point features, sensitivity to the excitonic binding energy parameter was limited and thus we held it to a constant value of 0.12, 0.23, and 0.18 eV for CP_{0x}^{ac}, CP_{1x}^{ac}, and CP_{0x}^b, respectively, as determined previously for room temperature.[12]

Temperature dependent energy parameters for critical points are shown in Fig. 3. The Bose-Einstein model as described by Viña *et al.* (Ref. 25) can be used to describe temperature dependence effects to render the shifts in energy parameters according to

$$E(T) = E_0 - \frac{\alpha P}{\exp(P/k_B T) - 1}, \tag{3}$$

where α is the phonon interaction strength and P is the phonon frequency as determined by temperature dependent energy shifts. We note that this equation is the result of an empirical derivation in which the symmetry of a given material is disregarded. Instead, it is thought that phonons contribute to the reduction of the band-to-band transitions as a spatially randomized ensemble characterized by the phonon energy rather than its polarization within a lattice. Recently, Sturm *et al.* (Ref. 19) applied this technique for low temperature generalized ellipsometry analysis of single crystalline β-Ga_2O_3. We also apply this model and extend it to our high temperature measurements.

The resulting lineshapes are shown as red solid lines in Fig. 3, and resulting parameters are given in Table III. We note that in the temperature range investigated, there is limited sensitivity to the parameter E_0; therefore, we have fixed this parameter to a value estimated from results published by Sturm *et al.* (Ref. 19). We find an average isotropic phonon

TABLE I. Best-match model calculated below-band-gap dielectric tensor elements and their Cauchy polynomial coefficients and temperature dependence parameter values according to Eq. (2) for monoclinic β-Ga_2O_3. Digits within parentheses denote the 90% confidence interval determined using the numerical uncertainties determined for each data point during the dielectric function tensor analysis.

	$\varepsilon_{1,xx}$	$\varepsilon_{1,yy}$	$\varepsilon_{1,zz}$	$\varepsilon_{1,xy}$
$\varepsilon_{\infty,ij}$	3.4(7)	3.5(5)	3.6(0)	–0.00(3)
A (10^{-5} C^{-1})	1(0)	1(2)	1(1)	–1.(9)
B (10^{-2} μm^2)	5.(3)	5.(9)	6.(6)	0.(1)
C (10^{-3} μm^4)	0.(6)	0.(4)	–(2)	–0.(1)
$\varepsilon_{\infty,ij}$	3.7(5)[a]	3.2(1)[a]	3.7(1)[a]	–0.0(8)[a]
$\varepsilon_{\infty,ij}$	3.479[b]	3.574[b]	3.626[b]	0.016[b]

[a]FIR-IR-GSE phonon analysis, Schubert *et al.*[18]
[b]Room temperature VIS-VUV GSE, Sturm *et al.*[10]

TABLE II. Parameter energy values determined from the eigendielectric displacement vector approach for the temperatures investigated in this work. Digits within parentheses denote 90% confidence determined from this analysis.

Temp.	CP_{0x}^{ac} E(eV)	CP_0^{ac} E(eV)	CP_{1x}^{ac} E(eV)	CP_1^{ac} E(eV)	CP_{0x}^b E(eV)	CP_0^b E(eV)
22 °C	4.9(2)	5.0(4)	5.1(7)	5.4(0)	5.4(6)	5.6(4)
50 °C	4.8(9)	5.0(1)	5.1(7)	5.4(0)	5.4(3)	5.6(1)
100 °C	4.8(6)	4.9(8)	5.1(4)	5.3(7)	5.3(9)	5.5(7)
150 °C	4.8(3)	4.9(5)	5.1(1)	5.3(4)	5.3(4)	5.5(2)
200 °C	4.8(1)	4.9(3)	5.0(7)	5.3(0)	5.3(2)	5.5(0)
250 °C	4.7(7)	4.8(9)	5.0(4)	5.2(7)	5.2(8)	5.4(6)
300 °C	4.7(5)	4.8(7)	4.5(0)	5.2(3)	5.3(2)	5.5(0)
350 °C	4.7(0)	4.8(2)	4.9(6)	5.1(9)	5.2(1)	5.3(9)
400 °C	4.6(6)	4.7(8)	4.9(2)	5.1(5)	5.1(9)	5.3(7)
450 °C	4.6(3)	4.7(5)	4.9(2)	5.1(5)	5.1(9)	5.3(7)
500 °C	4.5(9)	4.7(1)	4.8(6)	5.0(9)	5.2(0)	5.3(8)
550 °C	4.5(6)	4.6(8)	4.8(3)	5.0(6)	5.1(2)	5.3(0)

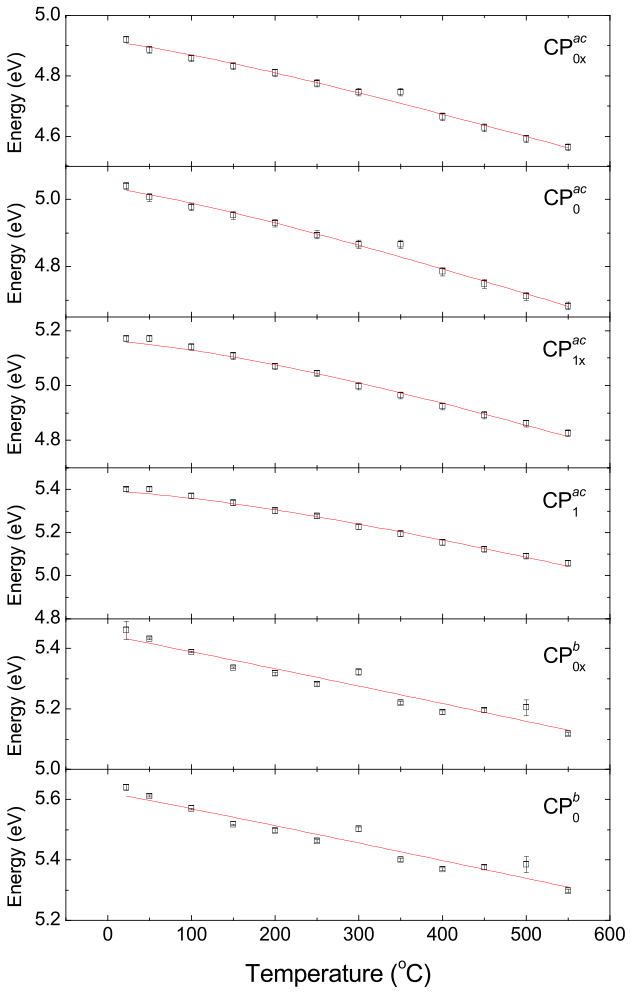

FIG. 3. Temperature dependence of energy parameters for critical points CP_{0x}^{ac}, CP_{0x}^{ac}, CP_{1x}^{ac}, CP_{1}^{ac}, CP_{0x}^{b}, CP_{0}^{b}. The red solid lines indicate the Bose-Einstein model lineshape.

TABLE III. Parameter values determined from a Bose-Einstein model of temperature dependent parameter values. Digits within parentheses denote 90% confidence determined from this analysis.

CP	E_0 (eV)	α (unitless)	P (eV)	α (Ref. 19)[a]	P (Ref. 19)[a]
CP_{0x}^{ac}	4.949[b]	9.(6)	0.0(7)	10.5	0.050
CP_{0}^{ac}	5.069[b]	9.(6)	0.0(7)	10.5	0.050
CP_{1x}^{ac}	5.18[b]	1(2)	0.1(0)	10.5	0.050
CP_{1}^{ac}	5.41[b]	1(2)	0.1(0)	10.5	0.050
CP_{0x}^{b}	5.52[b]	(7)	0.0(3)	5.5	0.025
CP_{0}^{b}	5.7[b]	(7)	0.0(3)	5.5	0.025

[a]Parameter average values determined for the a-c plane and the b axis separately by Sturm *et al.*
[b]Ref. 19.

frequency to be approximately 0.067 eV (537.7 cm^{-1}) from all energy parameters for the transitions investigated. The arithmetic average of all (symmetry independent) LPP phonons found by Schubert *et al.* was found to be 507.5 cm^{-1},[18] which is in excellent agreement with the value found in the present study.

In summary, we present the dielectric function tensor elements of β-Ga_2O_3 from room temperature up to 550 °C. Further, we provide a description of the linear temperature dependence of the wavelength independent Cauchy coefficient to obtain the temperature effects on the anisotropic below-band-gap monoclinic dielectric tensor elements. Additionally, we determine shifts in eigendielectric vector displacement approach energy parameters due to changes in temperature and model these effects by utilizing a Bose-Einstein lineshape to determine average phonon frequency. This approach could be utilized for design of devices operating at elevated temperatures.

We thank K. Goto and A. Kuramata and Tamura Corp. for providing the samples studied in this investigation. This work was supported by the National Science Foundation (NSF) through the Center for Nanohybrid Functional Materials (EPS-1004094), the Nebraska Materials Research Science and Engineering Center (DMR-1420645), the Swedish Research Council (VR2013-5580), and the Swedish Foundation for Strategic Research (SSF, FFL12-0181 and RIF14-055). Partial financial support from NSF (CMMI 1337856, EAR 1521428) and J. A. Woollam Foundation is also acknowledged.

[1]R. Roy, V. G. Hill, and E. F. Osborn, J. Am. Chem. Soc. **74**, 719 (1952).
[2]H. H. Tippins, Phys. Rev. **140**, A316 (1965).
[3]M. Higashiwaki, K. Sasaki, A. Kuramata, T. Masui, and S. Yamakoshi, Appl. Phys. Lett. **100**, 013504 (2012).
[4]M. Higashiwaki, K. Sasaki, T. Kamimura, M. Hoi Wong, D. Krishnamurthy, A. Kuramata, T. Masui, and S. Yamakoshi, Appl. Phys. Lett. **103**, 123511 (2013).
[5]A. J. Green, K. D. Chabak, E. R. Heller, R. C. Fitch, M. Baldini, A. Fiedler, K. Irmscher, G. Wagner, Z. Galazka, S. E. Tetlak *et al.*, IEEE Electron Device Lett. **37**, 902 (2016).
[6]M. H. Wong, K. Sasaki, A. Kuramata, S. Yamakoshi, and M. Higashiwaki, IEEE Electron Device Lett. **37**, 212 (2016).
[7]J. Yang, S. Ahn, F. Ren, S. Pearton, S. Jang, J. Kim, and A. Kuramata, Appl. Phys. Lett. **110**, 192101 (2017).
[8]K. Konishi, K. Goto, H. Murakami, Y. Kumagai, A. Kuramata, S. Yamakoshi, and M. Higashiwaki, Appl. Phys. Lett. **110**, 103506 (2017).
[9]J. F. Wager, Science **300**, 1245 (2003).
[10]C. Sturm, J. Furthmüller, F. Bechstedt, R. Schmidt-Grund, and M. Grundmann, APL Mater. **3**, 106106 (2015).
[11]C. Sturm, R. Schmidt-Grund, C. Kranert, J. Furthmüller, F. Bechstedt, and M. Grundmann, Phys. Rev. B **94**, 035148 (2016).
[12]A. Mock, R. Korlacki, C. Briley, V. Darakchieva, B. Monemar, Y. Kumagai, K. Goto, M. Higashiwaki, and M. Schubert, Phys. Rev. B **96**, 245205 (2017).
[13]J. Furthmüller and F. Bechstedt, Phys. Rev. B **93**, 115204 (2016).
[14]N. Ueda, H. Hosono, R. Waseda, and H. Kawazoe, Appl. Phys. Lett. **70**, 3561 (1997).
[15]Y. Kokubun, K. Miura, F. Endo, and S. Nakagomi, Appl. Phys. Lett. **90**, 031912 (2007).
[16]T. Oshima, T. Okuno, N. Arai, N. Suzuki, S. Ohira, and S. Fujita, Appl. Phys. Express **1**, 011202 (2008).
[17]R. Suzuki, S. Nakagomi, and Y. Kokubun, Appl. Phys. Lett. **98**, 131114 (2011).
[18]M. Schubert, R. Korlacki, S. Knight, T. Hofmann, S. Schöche, V. Darakchieva, E. Janzén, B. Monemar, D. Gogova, Q.-T. Thieu *et al.*, Phys. Rev. B **93**, 125209 (2016).
[19]C. Sturm, R. Schmidt-Grund, V. Zviagin, and M. Grundmann, Appl. Phys. Lett. **111**, 082102 (2017).
[20]M. Schubert, Phys. Rev. Lett. **117**, 215502 (2016).
[21]H. Aida, K. Nishiguchi, H. Takeda, N. Aota, K. Sunakawa, and Y. Yaguchi, Jpn. J. Appl. Phys., Part 1 **47**, 8506 (2008).
[22]K. Sasaki, M. Higashiwaki, A. Kuramata, T. Masui, and S. Yamakoshi, J. Crystal Growth **378**, 591 (2013).
[23]K. Shimamura and E. Villora, Acta Phys. Pol., A **124**, 265 (2013).
[24]S. Geller, J. Chem. Phys. **33**, 676 (1960).
[25]L. Viña, S. Logothetidis, and M. Cardona, Phys. Rev. B **30**, 1979 (1984).